Engineered Science

RESEARCH PAPER

View Article Online

Flower-like Bismuth Metal-Organic Frameworks Grown on Carbon Paper as a Free-Standing Electrode for Efficient Electrochemical Sensing of Cd^{2+} and Pb^{2+} in Water

Xianmei Xiang, Fuping Pan and Ying Li*

In this work, a free-standing electrode composed of bismuth terephthalate metal-organic frameworks grown on carbon paper (BiMOF/CP) was successfully prepared by a facile one-pot hydrothermal method. Materials characterization revealed the formation of flower-like ultrathin nanosheets of BiMOF fully covering on the microfibers of carbon paper. The BiMOF/CP was applied in the electrochemical detection of Cd^{2+} and Pb^{2+} in water. The BiMOF/CP electrode exhibited superior sensing performance with a linear detection of Cd^{2+} and Pb^{2+} with low detection limits of 1.5 μg/L for Cd^{2+} and 2.7 μg/L for Pb^{2+}, respectively. The significantly enhanced sensing performance compared to bare carbon paper is attributed to the 3D hierarchical architecture of BiMOF and increased number of exposed surface sites, facilitating the adsorption of metals ions and electron transfer. The prepared novel materials will contribute to the development of cost-effective electrochemical sensors for heavy metal detection.

Keywords: Bismuth; Metal-organic frameworks; Free-standing electrode; Heavy metals detection; Electrochemistry

Received 24th May 2018, Accepted 29th June 2018

DOI: 10.30919/es8d736

1. Introduction

Heavy metals have been regarded as one of the most severe sources of environmental pollution due to their non-biodegradable properties in ecological systems, quick accumulation, and toxicity in human body.[1] Among many heavy metals, Cd^{2+} and Pb^{2+} are two important representatives which can change the molecular structure of proteins on living organisms.[2] Thus, developing a sensitive, rapid, and simple analytical method to accurately detect heavy metals is necessary. Several analytical techniques have been developed such as inductively coupled plasma mass spectrometry,[3–5] flameless atomic absorption spectrophotometry,[6] and atomic absorption spectroscopy.[7] However, these conventional sensing techniques are complicated, time-consuming, and expensive, making them not suitable for quick detection. In contrast, the electrochemical methods, especially the anodic stripping voltammetry,[8–11] have been widely recognized as convenient techniques for metal ions detection due to easy operation, low cost and fast response. However, the low sensitivity and selectivity commonly limit their applications in practice owing to the lack of electroactive materials. In this content, searching for high-performance electroactive materials with high surface area, enhanced adsorptive ability, and a large number of electroactive sites is a crucial requirement.[12,13]

Metal-organic frameworks (MOFs) made of metal ions or clusters and organic linkers through strong coordination have received considerable attention as new functional materials. Due to their valuable virtues of extremely high surface area, multiple porosity and sufficient adsorption sites,[14–17] they have been widely applied in many research fields including gas adsorption, storage and separation,[18] organic dyes adsorption,[19] and heavy metals adsorption and uptake.[20–22] Recently, MOF-based electrochemical systems are attracting much attention as a sensing platform.[17] Especially in the electrochemical detection of heavy metals, MOFs have emerged as a burgeoning class of porous electroactive materials with high sensitivity for the Pb^{2+} [20,23–25] and Cd^{2+}[15,16] detection. In addition, it is reported that the oxygen-containing functional groups on

Department of Mechanical Engineering, Texas A&M University, College Station, TX 77843, USA. E-mail: yingli@tamu.edu

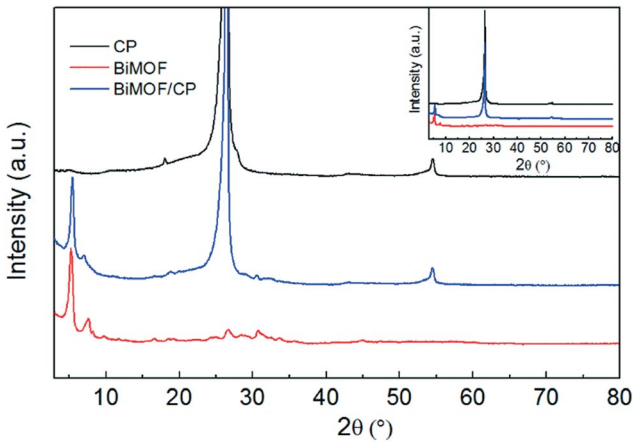

Fig. 1 XRD spectrum of pure CP, BiMOF and BiMOF/CP.

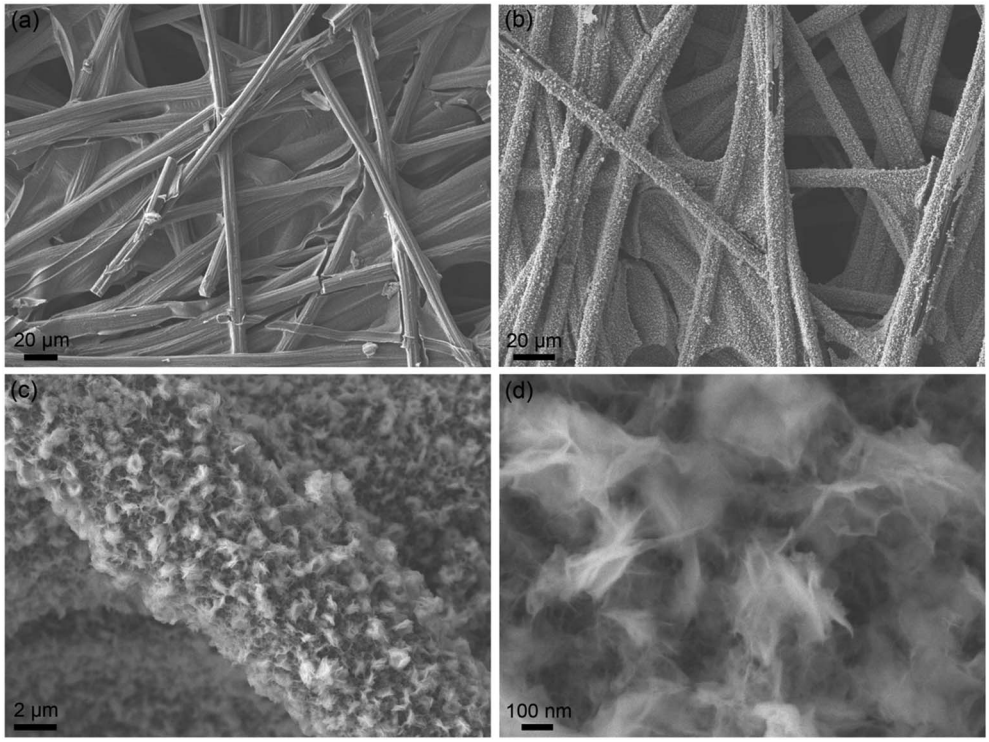

Fig. 2 SEM image of pure CP (a) and BiMOF/CP (b-d).

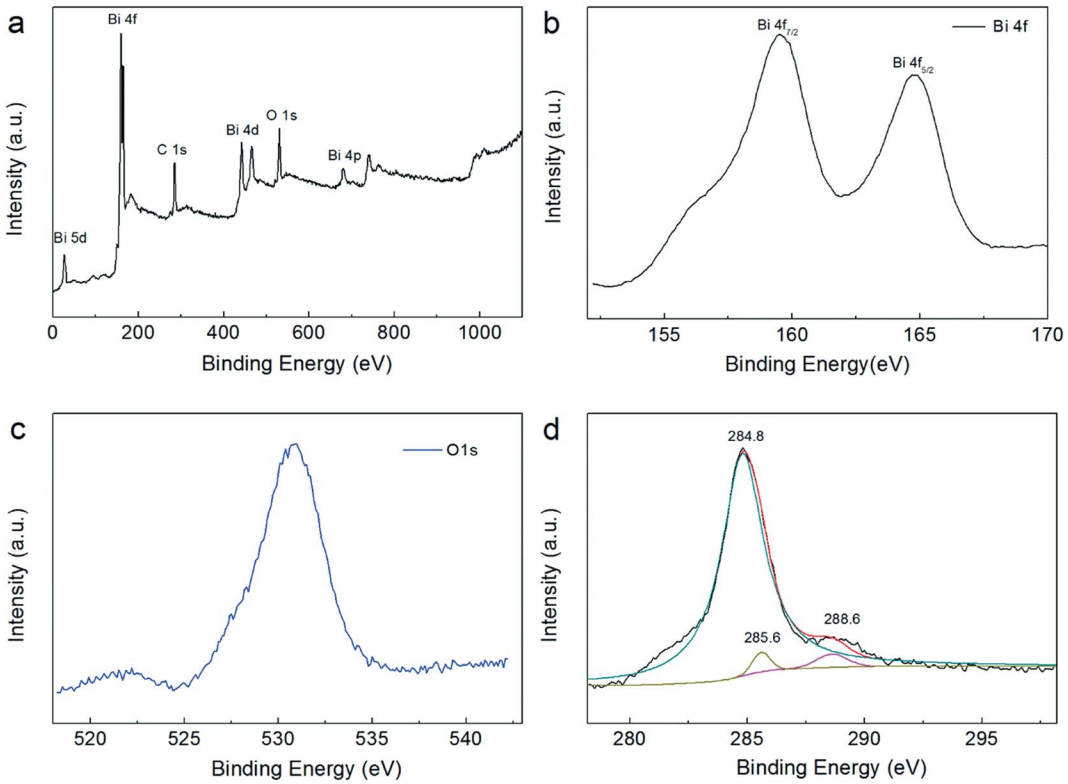

Fig. 3 XPS survey spectrum (a), Bi 4f (b) O1s (c), and C1s (d) of BiMOF/CP.

MOFs such as hydroxyl, carbonyl, carboxyl, can act as anchor sites to adsorb Cd^{2+} and Pb^{2+} to improve the analysis sensitivity.[26]

Bismuth is nontoxic, noncarcinogenic and relatively inexpensive, and thus bismuth and bismuth salts provide alternatives to mercury for heavy metal detection due to the attractive electrochemical features including reproducible stripping behavior and easy to form alloys with heavy metals.[27–31] Therefore, it is highly anticipated that the integration of excellent electrochemical features of bismuth with structure advantages of MOFs could be a promising candidate for electrochemical detection of heavy metals. On the other hand, the most reported electroactive materials for heavy metal ions detection are powder-type materials. In the practical electrochemical tests, the powder is required to be mixed with binders and then coated on the conductive substrates.[25,26,32–34] Mostly, the binders, which are usually insulators, may decrease the electrical conductivity of electrodes to have a negative effect on the performance.[35] In addition, there may be also new penalties arising from supplementary interfaces between the current collector and active material, as well as active materials themselves.[36,37] These high contact resistance and insufficient interactions will greatly decrease sensitivity. In this context, it is of great significance to develop free-standing electrodes consisting of electroactive materials being directly grown on three-dimensional (3D) conductive and robust substrates.

In this work, we report a free-standing electrode for electrochemical Cd^{2+} and Pb^{2+} detection by directly growing flower-like bismuth terephthalate MOF nanosheets on commercial carbon paper (BiMOF/CP) via a facile one-step hydrothermal process. The materials structure and composition have been systemically characterized via X-ray diffraction (XRD), scanning electron microscopy (SEM), and X-ray photoelectron spectroscopy (XPS), and Fourier-transform infrared spectroscopy (FT-IR). The BiMOF/CP was directly used for electrochemical detection of Cd^{2+} and Pb^{2+} individually and simultaneously.

2. Materials and Methods

2.1. Preparation of BiMOF/CP

The BiMOF/CP was synthesized according to a reported method.[38] Typically, 0.3225 g $Bi(NO_3)_3 \bullet 5H_2O$ was dissolved in 10 mL dimethylformamide (DMF), and 0.166 g terephthalic acid was dissolved in 7.5 ml DMF with magnetic stirring. Then, the solution of $Bi(NO_3)_3 \bullet 5H_2O$ was slowly added dropwise into the solution of terephthalic acid under stirring. Finally, the mixture was transferred into a 50 ml Teflon-lined stainless steel autoclave, and carbon paper (Toray Paper 060, 3.5 cm × 1.0 cm) was placed in the autoclave against the wall. The autoclave was maintained at 120 °C for 24 h and then cooled naturally to room temperature. The BiMOF/CP was obtained by thoroughly rinsing with deionized water and ethanol. Pure BiMOF precipitates were also collected from the solution in the autoclave as a reference for materials characterization purpose. Both BiMOF/CP and BiMOF were dried at 80 °C in a vacuum oven overnight for further use.

2.2. Physical Characterization

XRD patterns were recorded on a BRIKER D8 using Cu Kα irradiation at 45 kV and 40 mA diffracted beam monochromator. The surface morphology was obtained by scanning electron microscopy (SEM, JEOL JSM7500F) equipped with a cold cathode UHV field emission conical. XPS experiments were carried out in an ultrahigh vacuum using an Omicron's DAR 400 dual Mg/Al X-ray source. FTIR spectroscopy was recorded on Niclet iS50 (ThermoFisher Scientific).

2.3. Electrochemical measurements

All electrochemical measurements were carried out in a three-electrode system with an electrochemical workstation (Gamary Reference 3000). The BiMOF/CP or CP was directly used as working electrode. The auxiliary electrode was a platinum wire and the reference electrode was an Ag/AgCl electrode. The square wave anodic stripping voltammetry (SWASV) measurements were performed in a 50 mL beaker, containing 25 mL 0.1 M acetate buffer solution (pH 4.5) and known amounts of Cd^{2+} and Pb^{2+}. The pre-concentration step was carried out at -1.2 V for 240 s under stirring, when the target metals were deposited on the surface of the electrode. After a 10 s equilibration period, the SWASV potential scan was carried out from -1.2 V to -0.35 V with a frequency of 25 Hz, step increment of 4 mV and amplitude of 25 mV. All experiments were performed at room temperature under atmospheric conditions.

3. Results and discussion

3.1. Characterization of as-prepared BiMOF/CP

Figure 1 shows XRD patterns of pure CP, BiMOF and BiMOF/CP. Pure CP had two major diffraction peaks at 26.5° and 54.8°. BiMOF

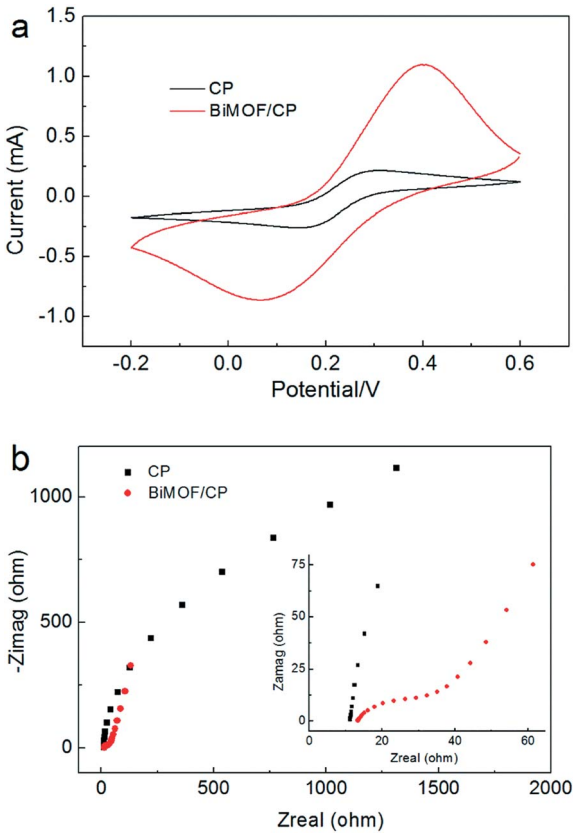

Fig. 4 (a) Cyclic voltammograms response and (b) electrochemical impedance spectra of CP and BiMOF/CP in 1.0 mM potassium hexacyanoferrate solution containing 0.5 M KCl.

exhibited high crystallinity with five main diffraction peaks at 5.3°,7.6°, 16.7°, 26.6° and 30.7°, which are consistent with the reported XRD pattern of BiMOF.[38] As for BiMOF/CP, it had the same four peaks at 5.3°, 7.6°, 16.7° and 30.7° as found in BiMOF, as well as two peaks at 26.5° and 54.8° as found in pure CP, suggesting the successful growth of BiMOF on CP.

The surface morphology and microstructure of BiMOF/CP were further investigated by SEM. As displayed in Figure 2a, pure CP exhibited a fiber structure with a smooth surface and a diameter around 10 μm. Figures 2b-d are SEM images of the as-prepared BiMOF/CP composite. It can be clearly seen that carbon fibers were fully and homogeneously covered with a dense coating (Figure 2b). In the magnified SEM images (Figures 2c-d), the flower-like structure of BiMOF was clearly observed, which was composed of ultrathin nanosheets. These nanosheets were interpenetrated and intertwined together to construct a 3D hierarchical architecture, making each layer of the flower-like structure accessible to the electrolyte.

In order to determine the composition and chemical states of BiMOF/CP, XPS characterization was performed. According to the XPS survey spectrum (Figure 3a), the presence of Bi, C, and O elements are confirmed. The high-resolution Bi 4f spectrum (Figure 3b) shows two individual peaks at 159.5 and 164.8 eV, which are Bi $4f_{7/2}$ and Bi $4f_{5/2}$, respectively. The Bi $4f_{7/2}$ reveals a trivalent oxidation state for bismuth.[39] The O 1s spectrum shows a peak at the binding energy of 530.8 eV (Figure 3c), suggesting the O is coordinated with Bi.[38] As shown in Figure 3d, the C 1s spectrum can be divided into three main peaks. The peak at binding energy of 284.8 eV is assigned to C-C bond, and the peaks at 285.6 and 288.6 eV are attributed to the aryl carbon from the benzene ring and carboxylate carbon of carboxylic acid. While for the pure CP, shown in Figure S1, there are only two elements, C and O. The C 1s shows one peak at 284.8 eV, and the O 1s shows one peak at 532.4 eV attributed to the adsorbed H_2O molecules. These results confirm that the BiMOF induces abundant Bi and O-containing functional groups, which could function as deposition sites of heavy metal ions to increase the detection sensitivity.[26,40,41]

The BiMOF/CP was further characterized by FT-IR spectroscopy. As shown in Figure S2, BiMOF/CP showed the same peaks compared to BiMOF with almost no shift in absorption band. The absorption peaks at near 1538 and 1382 cm^{-1} are assigned to the asymmetric and symmetric stretching vibration of the carboxylate group, respectively. The adsorption bands at 821 and 743 cm^{-1} are related to the out-of-plane ring C-H bending vibration of the terephthalate acid.[25] In addition, the band at 1698 cm^{-1} can be assigned to the C=O stretching vibration of aromatic carboxylic acids.[31] Furthermore, the bands at 1018 and 743 cm^{-1} can be assigned to the vibration of benzene rings.

The electrochemical characteristics of BiMOF/CP was first investigated in 1.0 mM potassium hexacyanoferrate ($K_3[Fe(CN)_6]$) solution containing 0.5 M KCl. As shown in the cyclic voltammetry (CV) curves (Fig. 4a), reversible redox peaks were obtained at pure CP with lower peak currents. After growing BiMOF, the composite electrode

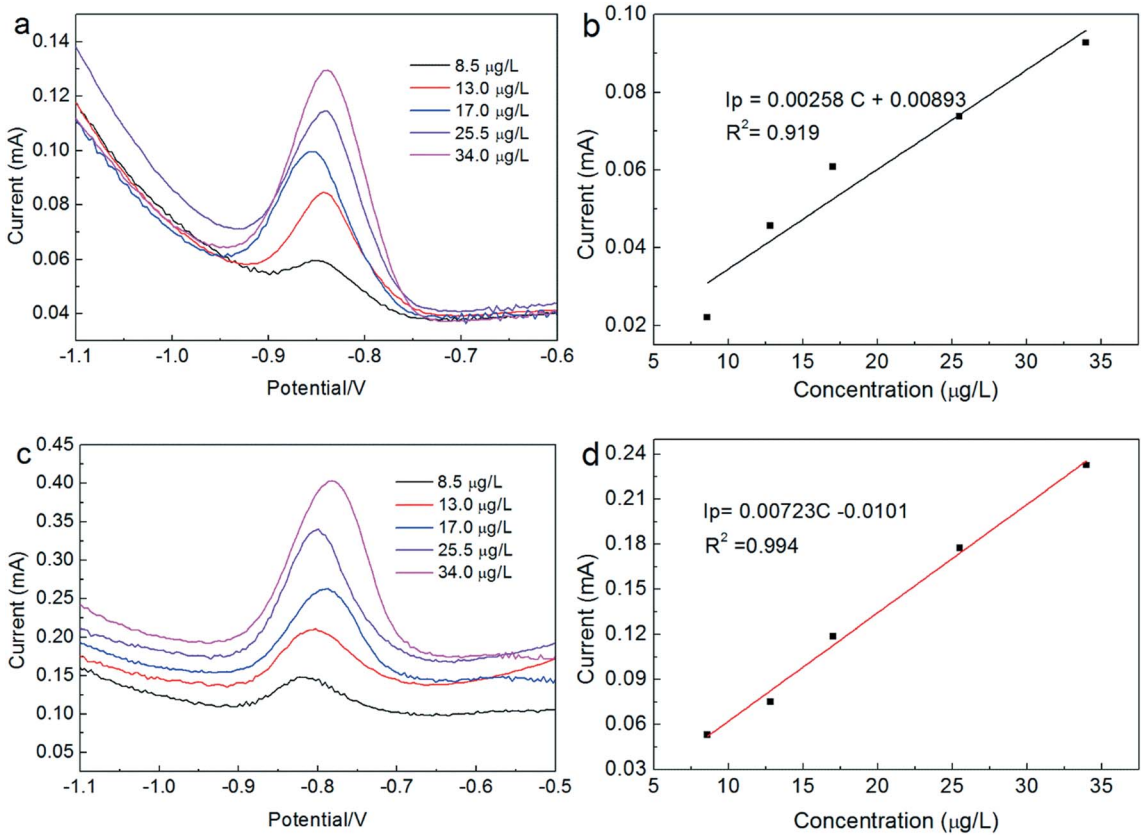

Fig. 5 SWSV curves of CP (a) and BiMOF/CP (c) with different concentrations of Cd^{2+} in the range from 8.5 to 34 μg/L, and the plots of stripping peak current vs. Cd^{2+} concentration for CP (b) and BiMOF/CP (d).

showed significant increase in anodic and cathodic currents, which might be resulted from the larger specific area and 3D hierarchical architecture of BiMOF that accelerated the electron transfer. The electrochemical impedance spectroscopy (EIS) was also carried out to explore the electron transfer process. As shown in Figure 4b, EIS curve of BiMOF exhibits a semicircular section in the high frequency zone and a linear section in the low frequency zone. The diameter of the semicircular is related to the electron transfer resistance (R_{CT}) reflecting the kinetic rates in the electrochemical reaction.[2,13,15,42] Generally, a bigger diameter means a larger R_{CT} and thus a slower reaction rate. Obviously, BiMOF/CP shows a significantly smaller R_{CT} of 29 Ω than that of pure CP (810 Ω), suggesting that BiMOF modification endowed CP with enhanced charge transfer property. This can be attributed to the 3D porous nanosheet structure of as-grown BiMOF, which provides enlarged specific surface area and therefore boosts the electron transfer.

3.2. Optimization of the pre-concentration conditions

There was no doubt that the deposition potential and pre-concentration time could affect the deposition amount of targeted metal ions on the electrode surface, which can affect the sensitivity and detection limit. In order to optimize the pre-concentration conditions, a 0.1 M HAc-NaAc solution containing 0.15 μM of Cd^{2+} or Pb^{2+} was used as the model sample, and various deposition potentials and pre-concentration times were tried to correlate with the sensing performance. It is found that the signal currents of Cd^{2+} and Pb^{2+} increased with the deposition potential from -1.0 to -1.4 V (Figure S3) but the rate of increase slowed down above -1.2 V. Similarly, the signal currents increased with increasing pre-concentration time from 120 to 360 s (Figure S4) but the rate of increase slowed down above 240 s. Because a higher deposition potential or a longer pre-concentration time leads to a higher operation cost, we chose -1.2 V deposition potential and 240 s pre-concentration time as the optimal values which were applied in the following experiments.

3.3. Individual and simultaneous detection of Cd^{2+} and Pb^{2+}

Under the optimized pre-concentration conditions (-1.2 V deposition potential and 240 s pre-concentration time), the analytical performance of BiMOF/CP composite electrode was first tested for the detection of Cd^{2+} and Pb^{2+} individually at different metal concentrations using a SWSV method. CP was also tested as a reference. The results of voltammograms and calibration plots for individual analyses are shown in Figure 5 for Cd^{2+} and Figure 6 for Pb^{2+}. It is observed that BiMOF/CP showed well-defined peaks toward Cd^{2+} and Pb^{2+} detection, and the signal current increased with increasing Cd^{2+} and Pb^{2+} concentration from 8.5 to 34 μg/L. Note that the currents on BiMOF/CP are much larger than those of pure CP, indicating the enhanced sensitivity. The peak currents and concentrations of metal ions exhibited a favorable linear relation over the range from 8.5 to 34 μg/L with a correlation coefficient of 0.994 for Cd^{2+} (Figure 5c) and a correlation coefficient

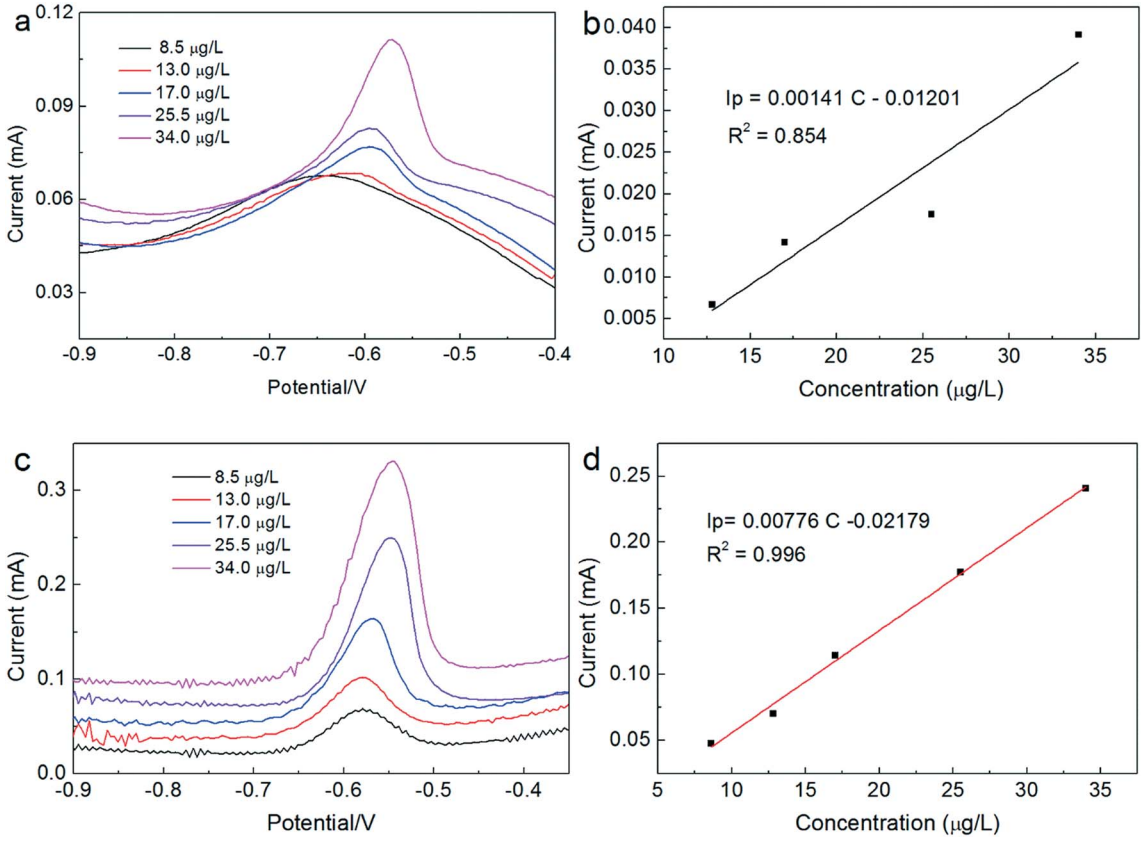

Fig. 6 SWSV curves of CP (a) and BiMOF/CP (c) with different concentrations of Pb^{2+} in the range from 8.5 to 34 μg/L, and the plots of stripping peak current vs. Pb^{2+} concentration for CP (b) and BiMOF/CP (d).

of 0.996 for Pb^{2+} (Figure 6c). Obviously, the pure CP exhibited relatively poor linear relationship toward Cd^{2+} (Figure 5b) and Pb^{2+} (Figure 6b) detection compared to BiMOF/CP. The detection limit can be calculated as three times the background noise, i.e. 3 × SD/S, where SD is the standard deviation of 5 measurements, and S is the slope of linearity.[43] From the calibration curves in Figure 5d and 6d, the detection limits for Cd^{2+} and Pb^{2+} on BiMOF/CP are calculated to be 2.6 μg/L and 2.1 μg/L, respectively. Therefore, we have demonstrated that BiMOF/CP composite electrode with well-defined stripping response could be successfully applied to the individual determination of Cd^{2+} and Pb^{2+}.

The reason for significant improvement in Cd^{2+} and Pb^{2+} detection on BiMOF/CP compared to pure CP can be attributed to the favorable composition and structure of BiMOF. On one hand, BiMOF synthesized from $Bi(NO_3)_3 \bullet 5H_2O$ and terephthalic acid had Bi and oxygen-containing groups (Figure 3). These species have been demonstrated to be the main deposition sites for the reduction of metal ions to metal in the electrochemical pre-concentration step.[26,40,41] By contrast, the lack of functional sites on pure CP leads to the low accumulated amounts of heavy metal, thus giving rise to weak signal currents. On the other hand, compared to the smooth surface of pure CP, the BiMOF showed a three-dimensional ultrathin nanosheet architecture, which made a great contribution to increase exposed surface area and sites for loading more heavy metal and facilitate the charge transfer to boost the heavy metal deposition and stripping. Therefore, enhanced sensitivity for Cd^{2+} and Pb^{2+} detection was achieved on BiMOF-modified CP.

Simultaneous electrochemical detection of Cd^{2+} and Pb^{2+} was also performed in the same condition as the individual detection experiment, and the SWASV curves and corresponding calibration plots are presented in Figure 7. The BiMOF/CP composite electrode exhibited good sensitivity and selectivity toward Cd^{2+} and Pb^{2+} detection. The signal currents increased with increasing Cd^{2+} and Pb^{2+} concentrations from 8.5 to 34 μg/L, which were much higher than pure CP. In addition, a linear current was obtained on BiMOF/CP for Cd^{2+} (Figure 7c) and Pb^{2+} (Figure 7d). The limits of the detection for Cd^{2+} and Pb^{2+} were determined to be 1.5 μg/L and 2.7 μg/L, respectively. The drinking water safety standard is 5.0 μg/L for Cd^{2+} and 10.0 μg/L for Pb^{2+} as defined by the U.S. Environmental Protection Agency (USEPA). Thus, the detection limit and sensitivity obtained by the BiMOF/CP electrode meet the USEPA requirements for Cd^{2+} and Pb^{2+} detection in clean drinking.

The interference investigation was also carried out to investigate the selectivity of the BiMOF/CP for Cd^{2+} and Pb^{2+} detection. The As^{3+}, Zn^{2+}, Cu^{2+}, Hg^{2+} and Ni^{2+} were selected as referenced metal ions. We conducted measurements of Cd^{2+} (17 μg/L) and Pb^{2+} (17 μg/L) in the presence of one of the five interfering metals ions (34 μg/L). As shown in Figure S5, there were no additional signal peaks found for the five interfering metal ions, and the positions of the Cd^{2+} and Pb^{2+} peaks were preserved. The result indicates the high selectivity of our electrode

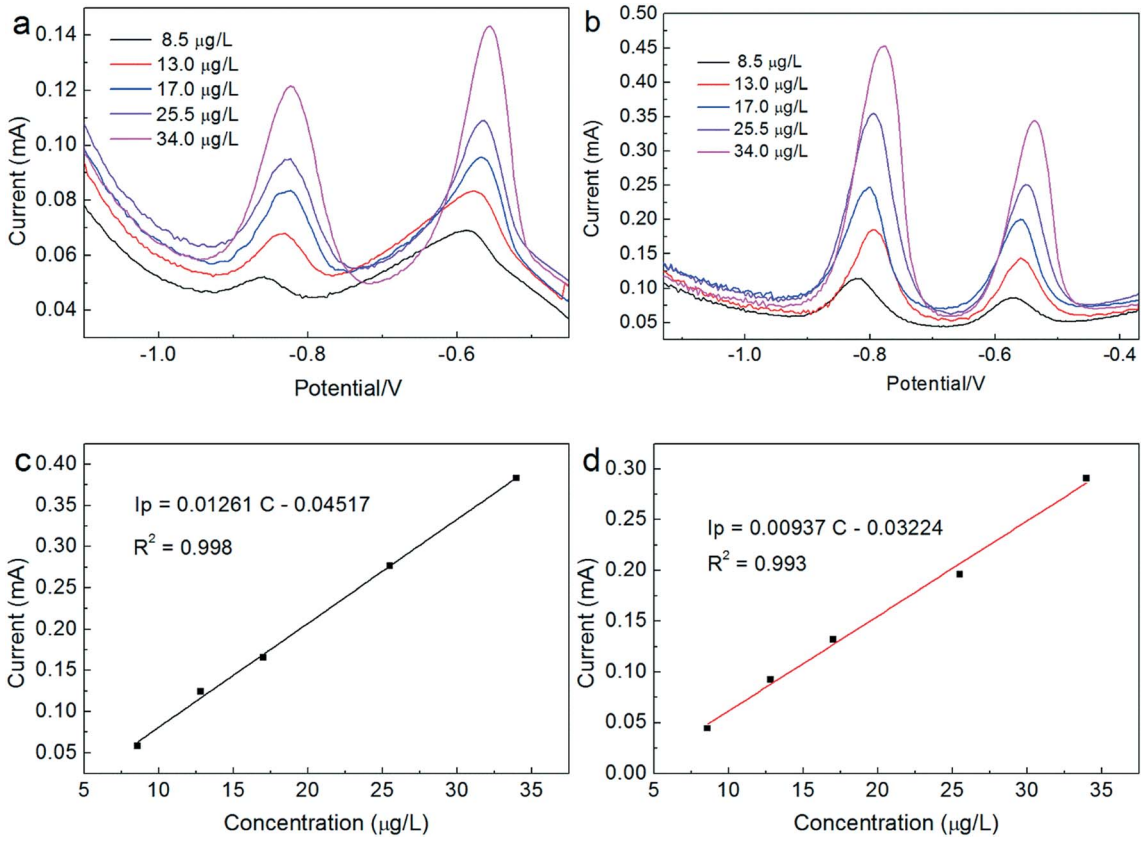

Fig. 7 SWSV curves for CP (a) and BiMOF/CP (b) with different concentrations of Cd^{2+} and Pb^{2+}, and the plots of stripping peak current vs. Cd^{2+} concentration (c) and Pb^{2+} concentration (d).

for Cd^{2+} and Pb^{2+} detection. However, the addition of interfering metals reduced the current signals for Cd^{2+} and Pb^{2+} to a various extent, which lowers the detection sensitivity of Cd^{2+} and Pb^{2+}. In practical applications, the interferences from other metal ions could be eliminated by applying a standard addition method,[20] so that more accurate detection of Cd^{2+} and Pb^{2+} can be achieved.

4. Conclusion

In summary, flower-like BiMOF has been successfully grown on carbon paper via a facile one-pot hydrothermal method for the detection of heavy metals. As a free-standing electrode, the resulting BiMOF/CP exhibited an outstanding electrochemical sensing performance toward Cd^{2+} and Pb^{2+} detection individually or simultaneously with low detection limits and high sensitivity. The enhanced performance was associated with the 3D porous structure constructed by ultrathin nanosheets with high surface area and sufficient exposure and homogenous distribution of active sites. Benefiting from facile preparation and high performance, the free-standing BiMOF/CP will be a potential electrode for constructing portable electrochemical sensors for heavy metal detection.

Conflict of interest

There are no conflicts to declare.

Acknowledgements

This work was supported by the Water Research Seed Grant of Texas A&M Engineering Experiment Station and Texas A&M University College of Engineering. We thank Wei Deng for performing SEM analysis and Dr. Chao Li and Xuhui Feng (Texas A&M University) for worthwhile discussions.

References

1 J. Barton, M.B.G. García, D.H. Santos, P. Fanjul-Bolado, A. Ribotti, M. McCaul, D. Diamond and P. Magni, *Microchim. Acta*, 2016, **183**, 503–517.
2 B. Petovar, K. Xhanari and M. Finšgar, *Anal. Chim. Acta*, 2018, **1004**, 10–21.
3 A.A. Ammann, *Anal. Bioanal. Chem.*, 2002, **372**, 448–452.
4 M. Bettinelli, G. Beone, S. Spezia and C. Baffi, *Anal. Chim. Acta*, 2000, **424**, 289–296.
5 M.B. Krishna and J. Arunachalam, *Anal. Chim. Acta*, 2004, **522**, 179–187.
6 T. Daşbaşı, Ş. Saçmacı, N. Çankaya and C. Soykan, *Food Chem.*, 2016, **203**, 283–291.
7 E.L. Silva and P. dos Santos Roldan, *J. Hazard. Mater.*, 2009, **161**, 142–147.
8 C. Ariño, N. Serrano, J.M. Díaz-Cruz and M. Esteban, *Anal. Chim. Acta*, 2017, **990**, 11–53.
9 G.M. Alves, L.S. Rocha and H.M. Soares, *Talanta*, 2017, **175**, 53–68.
10 U. Injang, P. Noyrod, W. Siangproh, W. Dungchai, S. Motomizu and O. Chailapakul, *Anal. Chim. Acta*, 2010, **668**, 54–60.
11 Y. Lu, X. Liang, C. Niyungeko, J. Zhou, J. Xu and G. Tian, *Talanta*, 2018, **178**, 324–338.
12 H. Lv, Z. Teng, C. Wang and G. Wang, *Sens. Actuators. B Chem.*, 2017, **242**, 897–903.
13 H.I. Maarof, M.A. Ajeel, W.M.A.W. Daud and M.K. Aroua, *Electrochim. Acta*, 2017, **249**, 96–103.
14 C. Yu, Z. Shao and H. Hou, *Chem. Sci.*, 2017, **8**, 7611–7619.
15 Y. Wang, L. Wang, W. Huang, T. Zhang, X. Hu, J.A. Perman and S. Ma, *J. Mater. Chem. A*, 2017, **5**, 8385–8393.
16 M. Roushani, A. Valipour and Z. Saedi, *Sens. Actuators. B Chem.*, 2016, **233**, 419–425.
17 Z. Wang, H. Yu, J. Han, G. Xie and S. Chen, *Chem. Commun.*, 2017, **53**, 9926–9929.
18 J. An and N.L. Rosi, *J. Am. Chem. Soc.*, 2010, **132**, 5578–5579.
19 E. Haque, J.W. Jun and S.H. Jhung, *J. Hazard. Mater.*, 2011, **185**, 507–511.
20 Y. Wang, Y. Wu, J. Xie and X. Hu, *Sens. Actuators. B Chem.*, 2013, **177**, 1161–1166.
21 Y. Peng, H. Huang, Y. Zhang, C. Kang, S. Chen, L. Song, D. Liu and C. Zhong, *Nat. Commun.*, 2018, **9**, 187.
22 Y. Zhang, Z. Xie, Z. Wang, X. Feng, Y. Wang and A. Wu, *Dalton Trans.*, 2016, **45**, 12653–12660.
23 H. Guo, Z. Zheng, Y. Zhang, H. Lin and Q. Xu, *Sens. Actuators. B Chem.*, 2017, **248**, 430–436.
24 H. Guo, D. Wang, J. Chen, W. Weng, M. Huang and Z. Zheng, *Chem. Eng. J.*, 2016, **289**, 479–485.
25 F. Cai, Q. Wang, X. Chen, W. Qiu, F. Zhan, F. Gao and Q. Wang, *Biosens. Bioelectron.*, 2017, **98**, 310–316.
26 L. Li, D. Liu, A. Shi and T. You, *Sens. Actuators. B Chem.*, 2018, **255**, 1762–1770.
27 Z. Lu, J. Zhang, W. Dai, X. Lin, J. Ye and J. Ye, *Microchim. Acta*, 2017, **184**, 4731–4740.
28 S. Lee, S. Bong, J. Ha, M. Kwak, S.-K. Park and Y. Piao, *Sens. Actuators. B Chem.*, 2015, **215**, 62–69.
29 J. Wang, *Electroanal.*, 2005, **17**, 1341–1346.
30 C. Hao, Y. Shen, J. Shen, K. Xu, X. Wang, Y. Zhao and C. Ge, *Microchim. Acta*, 2016, **183**, 1823–1830.
31 M. Feyand, E. Mugnaioli, F. Vermoortele, B. Bueken, J.M. Dieterich, T. Reimer, U. Kolb, D. De Vos and N. Stock, *Angew. Chem. Int. Ed.*, 2012, **51**, 10373–10376.
32 Y. Wei, R. Yang, X.-Y. Yu, L. Wang, J.-H. Liu and X.-J. Huang, *Analyst*, 2012, **137**, 2183–2191.
33 X. Li, H. Zhou, C. Fu, F. Wang, Y. Ding and Y. Kuang, *Sens. Actuators. B Chem.*, 2016, **236**, 144–152.
34 M. Mališić, A. Janošević, B.Š. Paunković, I. Stojković and G. Ćirić-Marjanović, *Electrochim. Acta*, 2012, **74**, 158–164.
35 X. Xie, K. Kretschmer, J. Zhang, B. Sun, D. Su and G. Wang, *Nano Energy*, 2015, **13**, 208–217.
36 P.-L. Taberna, S. Mitra, P. Poizot, P. Simon and J.-M. Tarascon, *Nat. Mater.*, 2006, **5**, 567.
37 T. Han, J. Jin, C. Wang, Y. Sun, Y. Zhang and Y. Liu, *Nanomaterials*, 2017, **7**, 40.
38 X. Zhao, X. Xiong, X. Chen, J. Hu and J. Li, *Appl. Organomet. Chem.*, 2016, **30**, 304–310.
39 L. Wu, J. Bi, Z. Li, X. Wang and X. Fu, *Catal. Today*, 2008, **131**, 15–20.
40 J. Wang, W. Zhang, X. Yue, Q. Yang, F. Liu, Y. Wang, D. Zhang, Z. Li and J. Wang, *J. Mater. Chem. A*, 2016, **4**, 3893–3900.
41 P. Niu, C. Fernández-Sánchez, M. Gich, C. Navarro-Hernández, P. Fanjul-Bolado and A. Roig, *Microchim. Acta*, 2016, **183**, 617–623.
42 Q. Jiang, Y.-P. Yeh, N. Lu, H.-W. Kuo, M. Lesslie and T. Xu, *J. Renew. Sust. Energ.*, 2016, **8**, 013701.
43 R. Karthik and S. Thambidurai, *J. Alloys Compd.*, 2017, **715**, 254–265.